

Nanoscale

Accepted Manuscript



This is an *Accepted Manuscript*, which has been through the Royal Society of Chemistry peer review process and has been accepted for publication.

Accepted Manuscripts are published online shortly after acceptance, before technical editing, formatting and proof reading. Using this free service, authors can make their results available to the community, in citable form, before we publish the edited article. We will replace this *Accepted Manuscript* with the edited and formatted *Advance Article* as soon as it is available.

You can find more information about *Accepted Manuscripts* in the [Information for Authors](#).

Please note that technical editing may introduce minor changes to the text and/or graphics, which may alter content. The journal's standard [Terms & Conditions](#) and the [Ethical guidelines](#) still apply. In no event shall the Royal Society of Chemistry be held responsible for any errors or omissions in this *Accepted Manuscript* or any consequences arising from the use of any information it contains.



Journal Name

ARTICLE

Bio-nanoplatfoms based on carbon dots conjugating with F-substituted nano-hydroxyapatite for cellular imaging

Yafei Zhao,^a Liyi Shi,^a Jianhui Fang^b and Xin Feng^{a*}

Received 00th January 20xx,
Accepted 00th January 20xx

DOI: 10.1039/x0xx00000x

www.rsc.org/

Carbon dots (CDs) have shown great promise in versatile bioapplications due to their tunable optical properties and nontoxicity. For the first time, a rationally designed strategy was designed to construct new bio-nanoplatfoms based on carboxylic acid terminated CDs (CDs-COOH) conjugating with amino terminated F-substituted nano-hydroxyapatite (NFAP) via EDC/NHS coupling chemistry. The monodispersed NFAP nanorods were functionalized with *o*-phosphoethanolamine (PEA) to provide them with amino groups and render them hydrophilicity based on ligand exchange process. The CDs-COOH@PEA-NFAP conjugates exhibits bright blue fluorescence under UV illumination, excellent photostability and colloidal stability. Due to the low cytotoxicity and good biocompatibility as determined by methyl thiazolyl tetrazolium (MTT) assay, the CDs-COOH@PEA-NFAP conjugates were successfully applied as bio-nanoplatfoms to MCF-7 breast cancer cell for cellular imaging *in vitro*. More importantly, the functional CDs conjugating to NFAP provides an extended and general approach to construct different water-soluble NFAP bio-nanoplatfoms to be available for other easy-functional luminescent materials. Therefore, the green type nanoplatfoms may provide a prospective candidate for bioimaging or targeted biological therapy and drug delivery.

Introduction

Increasing interests in fluorescent bio-imaging have been fueled by the high sensitivity, full-color imaging capability, low cost, and nontoxic.¹⁻³ Due to the complexity of the biosystems, a promising fluorescence imaging agents are often required to have several key features with water solubility, good biocompatibility, low/nontoxic cytotoxicity and outstanding optical properties.^{4,5} In recent years, there have been blowout growths in the development and biomedical applications of semiconductor quantum dots (predominantly CdTe/CdSe QDs).⁶⁻⁸ However, despite the unique photophysical properties of QDs,⁹ such as tunable band gaps, broad absorption spectra, size-controlled fluorescence and high resistance against photobleaching,^{10,11} a vital limitation is commonly caused by inevitable heavy metals.^{12,13} So scientists have been tried to find benign/non-toxic alternatives.¹⁴ Compared with these conventional QDs, photoluminescent carbon dots (CDs) are

emerging as a new class of carbon nanomaterials that reveal prodigious potential for making crucial breakthrough of bioimaging and biosensing, resulting from the excellent biocompatibility, intriguing chemical and optical properties, as well as nontoxicity.^{1,15-21} It is obvious that this novel carbon nanomaterial is an excellent candidate to supersede traditional semiconductor QDs for cell imaging and other biological research.

Hydroxyapatite (HAP) and their F-substituted counterparts (FAP) are the main inorganic components in both bones and teeth and also natural biocompatible materials.²²⁻²⁴ Due to the quantum confinement effect,^{25,26} nano-sized HAP and FAP are widely used in catalyst, sensors, tissue engineering, biomedical fields, and environmental phosphorus recovery.²⁷⁻²⁹ Furthermore, nano-HAP and their counterparts have been successfully demonstrated to be efficient building blocks, biocompatible scaffolds or multifunctional bio-nanoplatfoms³⁰⁻³⁴ loading several fluorescence imaging agents for targeted drug delivery and therapy, such as QDs, silica,³⁵ gold nanoparticles,³⁶ Na(Y/Gd)F₄·Yb³⁺,Er³⁺ nanocrystals,³⁷ and Fe₃O₄ nanoparticles.³⁸ Hsieh *et al.*³⁹ reported that poisonous CdSe@ZnS QDs anchored on HAP surface served as a fluorescent labeling of osteoblast cell. Zhou *et al.*⁴⁰ also utilized low-toxicity Mn-doped ZnSe@ZnS QDs conjugated with F-substituted nano-hydroxyapatite (NFAP) for cell imaging. Remarkably, with the growing demand on nontoxic fluorescence alternatives, CDs with highly optical performances will play a leading role in the rapid expanding research focused on fluorescence imaging or labelling of biosystems.

^a Research Center of Nano Science and Technology, Shanghai University, Shanghai 200444, P. R. China. *Corresponding Author: fengxin@shu.edu.cn

^b Department of Chemistry, Shanghai University, Shanghai 200444, P. R. China. Electronic Supplementary Information (ESI) available: Experimental details of monodispersed NFAP and Cell incubation; Quantum yield measurements of CDs and CDs-COOH; PL spectra of CDs-COOH@PEA-NFAP conjugates with different weight ratios in Figure S1; Excitation-dependent PL spectra of CDs-COOH in Figure S2; FTIR spectra of the CDs, CDs-COOH and ClCH₂COONa in Figure S3; XPS spectra of CDs and CDs-COOH in Figure S4; XRD pattern of CDs-COOH, OA-NFAP and PEA-NFAP in Figure S5; Element analysis of OA-NFAP and PEA-NFAP in Figure S6; Photostability of CDs-COOH@PEA-NFAP conjugates irradiated with different excitation wavelengths (325, 345, 365, 385, and 405 nm) over a period of 3 h in Figure S7; Bright-field photos and dark-field photos of CDs, CDs-COOH, PEA-NFAP, CDs-COOH@PEA-NFAP in Figure S8. See DOI: 10.1039/x0xx00000x

Herein, a multifunctional bio-nanoplatform for bioimaging with outstanding photoluminescence, nontoxicity and biocompatibility based on CDs covalently grafted with NFAP was successfully assembled in which CDs acted as fluorescent imaging agents/probes. Monodispersed NFAP nanorods were synthesized based on a typical hydrothermal phase transfer and separation strategy and then functionalized with *o*-phosphoethanolamine (PEA) to provide them with functional amino groups and render them hydrophilicity. CDs were prepared by a facile one-step carbonization process from citric acid and ethylenediamine, subsequently functionalized with sodium chloroacetate to provide them with functional carboxyl groups. After covalent crosslinking, the biocompatible and nontoxic CDs-COOH@PEA-NFAP conjugates were investigated by carrying out a series of MTT assays with three different cell lines. Furthermore, the bio-nanoplatform was successfully applied for bioimaging of MCF-7 breast cancer cell. The conjugates with perfect biocompatible and excellent optical properties can be potentially used as a multifunctional nanoplatform for tissue engineering, bio-imaging, targeted drug or gene delivery applications.

Experimental details

2.1 Chemicals and materials

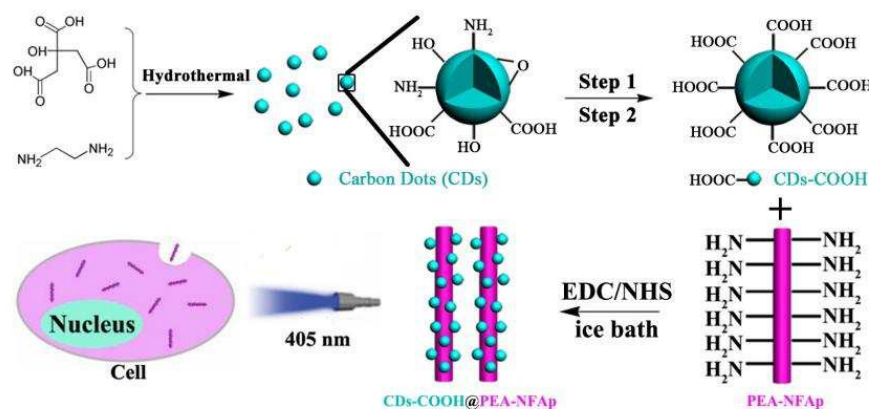
All the chemicals were used as received without further purification. Octadecylamine (90%), Calcium nitrate tetrahydrate ($\text{Ca}(\text{NO}_3)_2 \cdot 4\text{H}_2\text{O}$, 99%), Sodium fluoride (NaF, 99%), Sodium phosphate tribasic dodecahydrate ($\text{Na}_3\text{PO}_4 \cdot 12\text{H}_2\text{O}$, 98%), citric acid (99.5%), ethylenediamine (99.5%), Rhodamine B (99.0%), fluorescein isothiocyanate (FITC, 95%), Sodium chloroacetate (98%), and Sodium hydroxide (NaOH, 96%) were purchased from Aladdin. Oleic acid (OA, 90%), *o*-Phosphorylethanolamine (PEA), N-hydroxysuccinimide (NHS, 97%), 1-(3-dimethylamino-propyl)-3-ethylcarbodiimide Hydrochloride (EDC, 98%) were provided from Sigma Aldrich. Demonized water was used throughout.

2.2 Preparation of CDs and CDs-COOH

The photoluminescent CDs were synthesized by convenient one-step hydrothermal treatment with the typical procedures by Zhu *et al.*¹ In brief, citric acid (3.15 g) and ethylenediamine (1 mL) was dissolved in 30 mL deionized water. Subsequently, the solution was transferred into the poly(tetrafluoroethylene) (Teflon)-lined autoclave (50 mL) and heated at 200 °C for 5 h. After cooling to room temperature, the brown-black and transparent product was subjected to dialysis (molecular weight cutoff = 3500) against demonized water for 12 h in order to obtain pure CDs. Then, 100.0 mg of the as-synthesized CDs were dispersed in 50 mL of aqueous solution containing 5.0 g of NaOH and 5.0 g of $\text{ClCH}_2\text{COONa}$, followed by sonication at 900 W for 6 h. Interestingly, the color of the CDs suspensions changed from faint yellow to saffron yellow during the reaction, probably due to further reduction of the CDs under drastic alkaline conditions.⁴¹ After the treatments, the as-received CDs-COONa was neutralized with dilute HCl and dialysed against demonized water for overnight to remove any ions. Finally, the resultant was freeze-dried under vacuum at -50 °C before usage.

2.3 Preparation of hydrophilic and monodispersed PEA-NFAP nanorods

Monodispersed NFAP nanorods were successfully achieved *via* a previously reported hydrothermal route (ESI^+).⁴² Then, the hydrophobic monodispersed NFAP nanorods were treated with PEA to enhance the hydrophilic properties of NFAP based on ligand exchange according to a modified procedure described by Zhou *et al.*⁴⁰ 10 mg of oleic acid-capping NFAP nanorods was dispersed in 10 mL cyclohexane, and 10 mL aqueous solution containing of PEA (50 mg) was added under ice bath with violent stirring for 12 h. Subsequently, the hydrophobic NFAP was thoroughly transferred into the water solution owing to the ligand exchange from oleic acid to PEA. The lower NFAP aqueous solution was collected via a separating funnel and washed with demonized water for three times. After PEA modification, the additional amino groups immobilized onto the hydrophilic NFAP surface will accordingly provide further active sites to covalent link with CDs-COOH.



Scheme 1. Schematic illustration of the synthetic route of CDs-COOH@PEA-NFAP conjugates. Step 1: $\text{ClCH}_2\text{COONa}/\text{NaOH}$; Step 2: HCl.

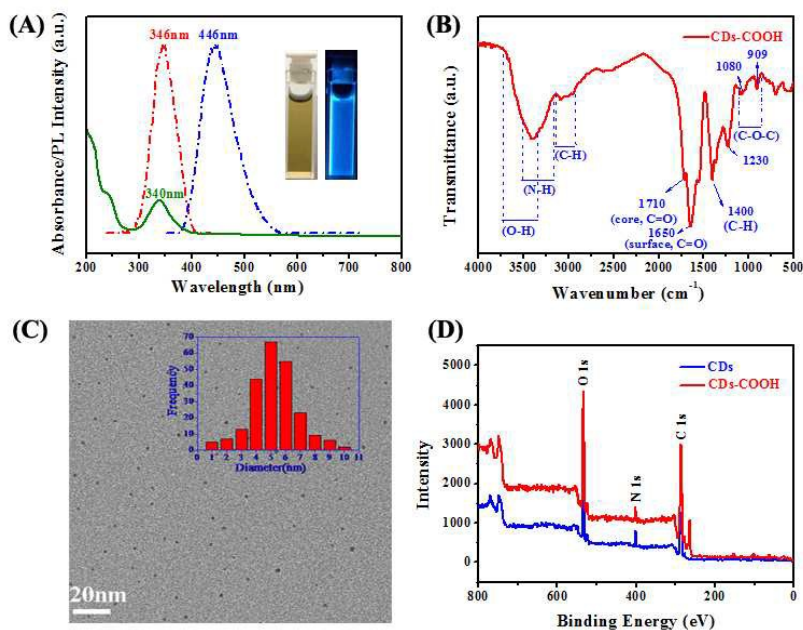


Figure 1. Characterization of the as-prepared CDs-COOH: (A) UV/Vis absorption (olive line), PL excitation (red dash dot), and emission (blue dash dot) spectra of CDs-COOH (0.1 mg mL^{-1}). Insets show photographs of CDs-COOH in aqueous solution under visible (left) and UV (right) light. (B) FTIR spectrum and (C) HRTEM image of CDs-COOH, inset: the distribution of nanoparticle sizes from TEM analysis. (D) XPS of the CDs and CDs-COOH.

2.4 Preparation of CDs-COOH@PEA-NFAP conjugates

In the present work, the CDs-COOH@PEA-NFAP conjugates were prepared at optimal weight ratios (2:3) giving the highest PL intensity (Figure S1). Briefly, the as-synthesized CDs-COOH (10 mL , 5 mg/mL) were dissolved in 5 mL ice-bathed Tris-HCl buffer (0.1 M , $\text{pH}=7.4$) containing 1-(3-dimethylamino-propyl)-3-ethylcarbodiimide hydrochloride (EDC, 40 mg) and N-hydroxysuccinimide (NHS, 20 mg) for 2 h to improve chemical reactivity. Then PEA-NFAP Tris-HCl (10 mL , 7.5 mg/mL) was added to the above solution in an ice bath under stirring, and the mixture was treated by ultrasonication in the ice bath for 12 h . The as-synthesized conjugates was washed three times and re-dispersed with Tris-HCl buffer. Then, the CDs-COOH@PEA-NFAP conjugates were stored at $4 \text{ }^\circ\text{C}$ for further use.

2.5 Cytotoxicity of the CDs-COOH@PEA-NFAP conjugates

The cellular cytotoxicity of CDs-COOH@PEA-NFAP conjugates on live cells was carried out a series of MTT 3-(4,5-dimethylthiazol-2-yl)-2,5-diphenyltetrazolium bromide) assays with three different cell lines.⁴³ MCF-7, HepG2, and Caco-2 cells were cultured using established procedures.^{19,44,45} These cells were cultured in 96-well assay plates at a density of 1×10^4 cells per well and incubated for 24 h . Then, The CDs-COOH@PEA-NFAP conjugates were import into the wells in a concentration range from 0 - $200 \text{ } \mu\text{g mL}^{-1}$. After another 24 h of incubation, the medium was removed and washed with PBS (phosphate-buffered) three times. Then, MTT ($10 \text{ } \mu\text{L}$, 5 mg mL^{-1}) solution was added to each well and the plate was incubated at $37 \text{ }^\circ\text{C}$ for 3 - 4 h . Next, $100 \text{ } \mu\text{L}$ dimethyl sulfoxide (DMSO) was re-added to each well to dissolve the dark blue formazan crystal, the assay plate was allowed to stand at room temperature for 2 h . The absorbance was measured

with a microplate reader (Biorad, USA) at a wavelength of 570 nm . The following formula was used to calculate the cell viability: cell viability (%) = (mean of the Abs. value of the treatment group/mean Abs. value of the Control) $\times 100\%$.

2.6 In vitro bioimaging of CDs-COOH@PEA-NFAP conjugates

Imaging of cells was performed with a confocal laser scanning microscope (excited at 405 nm). For imaging exogenous conjugates in live cells, MCF-7 cells were co-incubated with $100 \text{ } \mu\text{g mL}^{-1}$ CDs-COOH@PEA-NFAP RPMI1640 solution at $37 \text{ }^\circ\text{C}$ for 24 h and 48 h . Further, the cells were washed with phosphate buffered saline (PBS) to remove the excess conjugates.

2.7 Characterization

The average particle sizes and morphologies were characterized using a JEOL JEM-2010F low-to-high resolution transmission electron microscope (TEM) operated at 120 kV . Fourier transform infrared spectroscopy (FTIR) spectra were recorded in the spectral range from 4000 to 400 cm^{-1} with Thermo Nicolet 6700 spectrometer (Thermo Fisher Scientific, USA) by using the pressed KBr pellet technique. X-ray photoelectron spectroscopy (XPS) were acquired in a RBD upgraded PHI-5000C ESCA system (Perkin-Elmer) with Mg K_α radiation ($h_\nu = 1253.6 \text{ eV}$) or Al K_α radiation ($h_\nu = 1486.6 \text{ eV}$). UV-Vis spectra were recorded on a spectrophotometer (2500-PC, Shimadzu, Japan) at ambient temperature. Photoluminescence (PL) spectra were measured on a Shimadzu RF-5301 spectrophotometer. Cellular fluorescent image was recorded using a Confocal Laser Scanning Microscope (FV1000, Olympus Corporation, Japan). All data were expressed as the mean result \pm standard deviation (SD), and all figures were acquired from three independent experiments with consistent results.

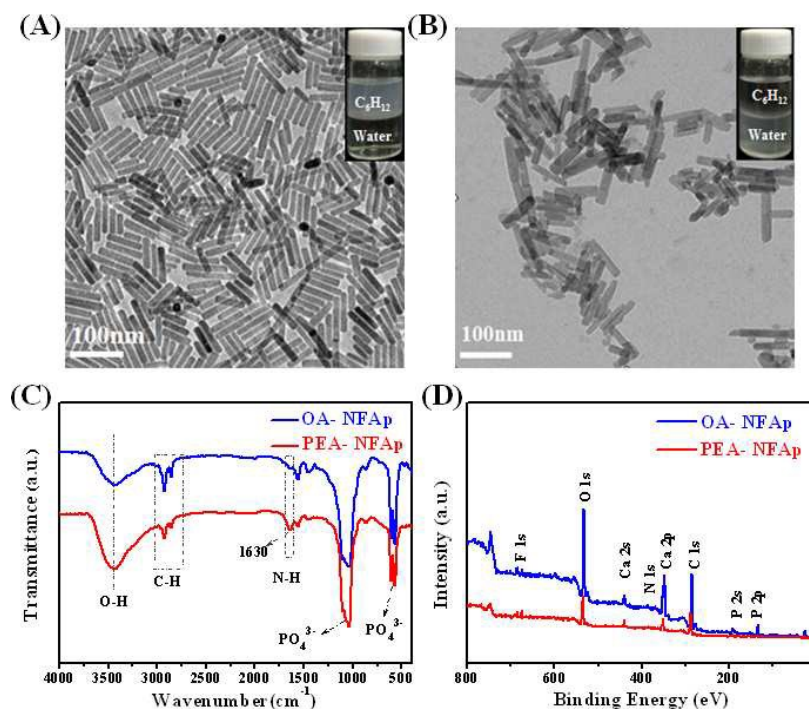


Figure 2. Characterization of the as-prepared NFAp nanorods: (A) TEM image of the hydrophobic NFAp nanorods; the inset shows nanorods dissolved in cyclohexane (upper) under room light; (B) TEM image of the hydrophilic NFAp nanorods; the inset shows nanorods dissolved in water (lower) under room light; (C) FTIR spectra of NFAp nanorods before and after PEA modification; and (D) XPS patterns of NFAp nanorods before and after PEA modification.

Results and Discussion

3.1 Characterization of CDs and CDs-COOH

CDs and the water-soluble, carboxyl-functionalized derivatives (CDs-COOH) were explored as novel fluorescence agents/probes, and the schematic illustration for the synthetic route of CDs and CDs-COOH was shown in Scheme 1. The hydrophilic CDs-COOH was surface modified according to a proposed procedure in the previous works^{41,46}. The primary groups (-OH/epoxy, amino) in the surface of CDs were successfully converted into carboxyl groups. The optical properties of the CDs-COOH were investigated by UV/Vis and PL spectroscopy. As demonstrated in the UV/Vis absorption spectrum (Figure 1A), the as-obtained CDs-COOH solution display two well-defined absorption feature centered at 240 nm and 340 nm, attributing to various $\pi-\pi^*$ transition (C=C) and $n-\pi^*$ transition (C=O). In the fluorescence spectra, the CDs-COOH has optimal excitation and emission wavelengths at 346 nm and 446 nm, exhibiting bright blue fluorescence under UV illumination (365 nm). In addition, CDs-COOH also shows obvious excitation-dependent PL behavior (Figure S2), similar to the previous literature.¹⁹ The quantum yield of CDs and CDs-COOH was determined to be 58% and 10.8% using quinine sulphate as a reference, respectively. Figure 1B displays the FT-IR spectrum of CDs-COOH. The three broad absorption bands at 3400-3800, 3200-3600 and 2900-3100 cm^{-1} were characteristic of O-H, N-H and C-H stretching vibration,

respectively. The others absorption bands were assigned as follows: 1650 cm^{-1} for C=O stretching vibration, 1400 cm^{-1} for C-H deformation peak, 1080 cm^{-1} and 909 cm^{-1} for epoxide, respectively. As a complement, the contrasting difference in FT-IR spectra evidently revealed the changes in the chemical functional groups on the CDs and CDs-COOH surface (Figure S3). After carboxylation reaction, a new peak at 1650 cm^{-1} appeared in the spectrum of the CDs-COOH compared to CDs and sodium chloroacetate, which was ascribed to the stretching vibration of the group -C=O that originated from the sodium chloroacetate. And both the disappearance of the two peak at 1080 cm^{-1} and 909 cm^{-1} corresponding to $\nu(-\text{COC}-)$ of the CDs. The N-H broad absorption bands (3200-3600 cm^{-1}) and the group $\nu(-\text{C=O})$ (1710 cm^{-1}) reduce sharply (the group may be hide in the CDs core region, firstly put forward) further significantly prove the conversion of the surface functional groups (e.g. hydroxyl, epoxide, amide) of CDs into -COOH group, resulting in high solubility in aqueous and reaction selectivity and specificity in the following bio-imaging experiment. N-doped, oxygen-containing CDs-COOH with -COOH groups on their surface also possess excellent water-solubility and predominant optical property, which will be explored as fluorescent agents/probes for biomedicine. XPS measurement was performed to identify the composition of the as-prepared CDs and CDs-COOH. As can be seen in Figure 1D, the XPS spectra of CDs and CDs-COOH show a predominant graphitic C_{1s} peak at ca. 284 eV, an O_{1s} peak at ca. 532 eV, and a pronounced N_{1s} peak at ca. 400 eV. In the high resolution XPS spectra (Figure S4), the C_{1s} peaks at 284.8, 286.3, 287.8, and

289.9 eV (Figure S4A) can be assigned to carbon in the form of C–C (sp^3), C–N (sp^3), C=O (sp^2), and O–C=O (sp^2), respectively. The N_{1s} peaks (Figure S4B) at 400.7 and 401.9 eV indicate that nitrogen exists mostly in the form of $(C)_3-N$ (sp^3) and N–H (sp^3), respectively. The O_{1s} peaks (Figure S4C) at 533.8 and 532.4 eV are associated with oxygen in the states of C=O and C–OH/C–O–C, respectively. The results are well consistent with FTIR measurements. It is obvious from TEM images (Figure 1C) that the uniform near-spherical nanoparticles with an average size of 5.1 ± 1.2 nm as estimated from statistical distributions. In addition, the XRD pattern of CDs-COOH (Figure S5A) shows a broad (002) peak centered at approximately 22° , which can be indexed as the graphite carbon.

3.2 Characterization of OA-NFAP and PEA-NFAP nanorods

HAp nanorods with excellent biocompatibility and bioresorbability are usually explored in the fields of tissue engineering, bio-medicine, etc. Uniform nano-sized fluorine-substituted HAp (NFAP) acted as a nanoplatform for potential applications in bioimaging was investigated. As shown in Figure 2A, uniform and well-dispersed NFAP nanorods were successfully achieved with a size of 85–135 nm in length and 10–20 nm in width. The OA-capping NFAP is easily dispersed in cyclohexane (inset of Figure 2A), attributed to the long alkyl chains of oleic acid adsorbed on the surface of the NFAP. The OA-capping super-hydrophobic surfaces of NFAP nanorods perhaps hamper their potential bio-application in hydrophilic environment. In order to obtain the hydrophobic/hydrophilic conversion, a simple strategy for converting hydrophobic NFAP nanorods into water-soluble and amino-functioned analogues by PEA via Ca–P coordination chemistry, resulting in the generation of free amino groups on the surface⁴⁰. Furthermore, the ligand-exchange route has no obvious adverse effects on the morphologies, phases and compositions of NFAP from TEM image (Figure 2B) and XRD patterns (Figure S5B). It can be clearly seen that the hydrophilic NFAP is well dispersed in water (inset of Figure 2B). The PEA-capping ligands on the surface of NFAP was identified by FT-IR spectra (Figure 2C) and XPS analysis (Figure 2D). Both OA-NFAP and PEA-NFAP exhibit a broad band at around 3400 cm^{-1} , corresponding to O–H stretching vibration. The transmission bands at 2930 and 2855

cm^{-1} were attributed to the asymmetric and symmetric stretching vibrations of methylene (CH_2), however, the peaks in the spectrum of the PEA-NFAP apparently decreased. In addition, a new peak at 1630 cm^{-1} in the spectrum of the PEA-NFAP is ascribed to the deformation vibration of the group N–H originated from the outer layer of PEA ligand. As previously reported,⁴⁰ XPS results of PEA-NFAP clearly support the FTIR measurements. The O_{1s} and N_{1s} peak heights apparently increase, while the C_{1s} decreases (Figure 2D). Moreover, for OA-NFAP and PEA-NFAP, the Ca/P atomic ratios in the solid are 1.32 and 1.28 (Figure S6), respectively. XPS analysis further verifies the interactions between PEA and NFAP. The result indicates that, for these two compositions, Ca^{2+} species of the NFAP may composite with PO_4^{3-} of the PEA.

3.3 Characterization of CDs-COOH@PEA-NFAP conjugates

The assembly of the CDs-COOH@PEA-NFAP conjugates was carried out via an EDC/NHS coupling chemistry^{40,47-49} (scheme 1). The morphology and structure of individual CDs-COOH@PEA-NFAP conjugates and PEA-NFAP nanorods were examined with HRTEM (Figure 3A and 3B). From Figure 3A, it can be clearly observed that CDs-COOH are uniformly distributed and combined with PEA-NFAP closely, similar to the well-dispersed sesame on hot dog, suggesting that the carboxyl-modified CDs have been well-bonded with NFAP through EDC/NHS coupling reaction. However, only the NFAP lattice can be detected from the HRTEM image of PEA-NFAP nanorods, the lattice spacing was observed with $d_{002}=0.347\text{ nm}$ (Figure 3B). The successful attachment of the CDs to NFAP was also illustrated by the UV/Vis absorption spectrum and FTIR spectra. The UV/Vis absorption spectra of the CDs-COOH and CDs-COOH@PEA-NFAP are shown in Figure 4A. Compared to PEA-NFAP, CDs-COOH@PEA-NFAP conjugates have a clearly absorption peak approx. 340 nm. Figure 4B shows the FTIR of the CDs-COOH@PEA-NFAP conjugates, a new peak at 1710 cm^{-1} appeared in the spectrum of the conjugates compared to PEA-NFAP, ascribed to the stretching vibration of the group C=O that originated from CDs (may be hide in the CDs core region). The FT-IR and UV/Vis spectrum characterization further confirmed that CDs-COOH was successfully conjugated to NFAP.

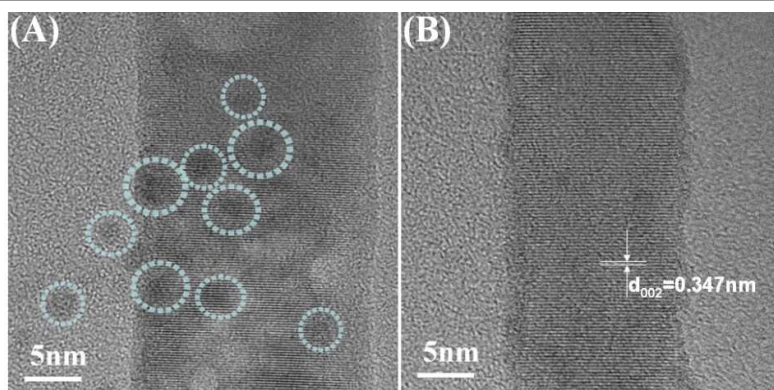


Figure 3. Morphological analysis of the as-prepared CDs-COOH@PEA-NFAP conjugates. HRTEM image of CDs-COOH@PEA-NFAP conjugates (A) and PEA-NFAP nanorods (B).

The photostability of the CDs-COOH@PEA-NFAP conjugates is an important feature for potential bio-applications. Herein, we exposed CDs-COOH@PEA-NFAP conjugates, fluorescein isothiocyanate (FITC), CdTe QDs, Rhodamine B irradiated with 365 nm excitation light for various time points. As shown in Figure 5A, the fluorescence of FITC was sharply quenched within 10 min under excitation owing to severe photobleaching, the CdTe QDs and Rhodamine B were more photostable, retaining 88% and 66% of the original PL intensity after 10 min excitation, But a striking decrease were obvious beyond the 30 min. By contrast, under approximately 70 min excitation, the PL intensity of all the as-synthesized CDs-COOH@PEA-NFAP decreased slightly, preserving over 90% of the initial intensity. In addition, under different excitations (325, 345, 365, 385, and 405 nm), the PL intensity of CDs-COOH@PEA-NFAP conjugates still maintained more than 90% of the initial value even after irradiation for 3 h (Figure S7). To further investigate the stability of CDs-COOH@PEA-NFAP conjugates in Tris-HCl buffer, the fluorescence spectra of CDs-COOH@PEA-NFAP were recorded over a period of 3 h (Figure 5B). The luminescence intensity of CDs-COOH@PEA-NFAP maintained more than 90% of its initial value when measured over a period of 180 min. It is further illustrated that the CDs-COOH@PEA-NFAP conjugates possess colloidal stability and

photostability, which is promising for the applications in physiology with no dissociation under physiological conditions. Furthermore, there was no obvious dissociation or aggregation of CDs-COOH@PEA-NFAP conjugates. Blue fluorescence can be detected by the bare eye under handheld UV Lamps at excitation wavelength of 365 nm (Figure S8).

3.4 *In vitro* cytotoxicity studies

The biocompatibility of CDs-COOH@PEA-NFAP conjugates was essential to be evaluated to investigate their potential biological application. Therefore, a series of standard methyl thiazolyl tetrazolium (MTT) assays with three different cell lines (MCF-7, HepG2, Caco-2) were carried out to evaluate the cytotoxicity. As shown in Figure 6, it can be shown that more than 94 % of all the cells can survive even after incubation of CDs-COOH@PEA-NFAP conjugates for 24 h with a concentration of $100 \mu\text{g mL}^{-1}$. In addition, even at a high dose of $200 \mu\text{g mL}^{-1}$, cell viabilities are still more than 90 %, demonstrating the non-toxicity of CDs-COOH@PEA-NFAP conjugates. Hence, the good biocompatibility makes CDs-COOH@PEA-NFAP conjugates potential application for cell imaging *in vitro* or drug delivery in biomedical applications as new bio-nanoplatforms.

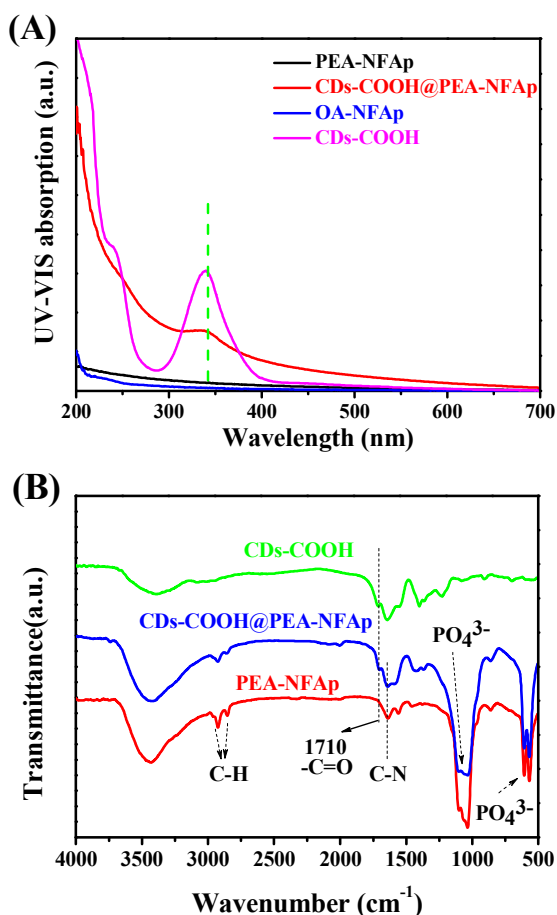


Figure 4. Characterization of the as-prepared CDs-COOH@PEA-NFAP conjugates. UV/Vis absorption spectra (A) and FT-IR spectra (B).

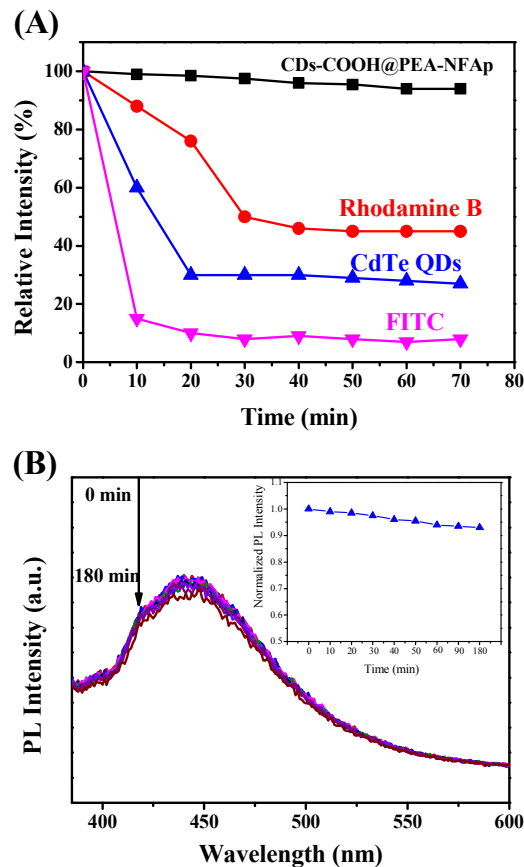


Figure 5. (A) Photostability comparison of Rhodamine B, CdTe QDs, FITC and CDs-COOH@PEA-NFAP conjugates under excitation wavelength with 365 nm ; (B) Photostability of CDs-COOH@PEA-NFAP conjugates irradiated with a laser excited at 365 nm at different time points (inset, normalized fluorescence intensity).

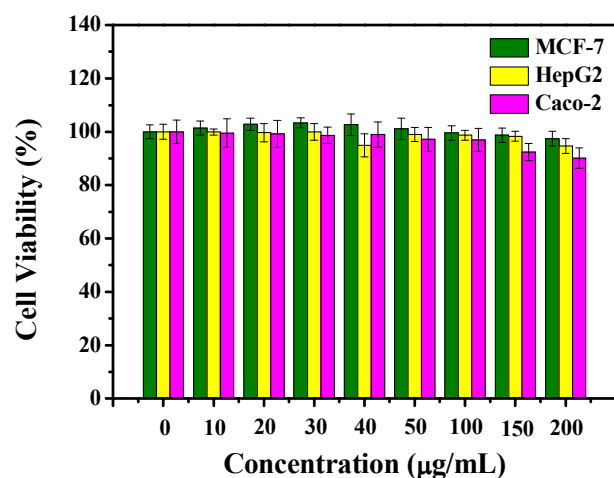


Figure 6. *In vitro* cell viabilities of three different cell lines (MCF-7, HepG2, Caco-2) incubated with CDs-COOH@PEA-NFAP conjugates at different concentrations (0, 10, 20, 30, 40, 50, 100, 150 and 200 $\mu\text{g mL}^{-1}$) for 24 h.

3.5 Cell imaging with the CDs-COOH@PEA-NFAP conjugates

Based on the excellent biocompatibility, hydrophilicity and blue emission under 405 nm excitation, the CDs-COOH@PEA-NFAP conjugates were used for bioimaging of MCF-7 breast cancer cell. Figure 7 shows the confocal imaging of MCF-7 cells incubated with CDs-COOH@PEA-NFAP conjugates ($100 \mu\text{g mL}^{-1}$) for 24 h and 48 h. The merged images and the bright-field images clearly confirm that the bright luminescence was localized in the cytosol region rather than merely staining the membrane surface. They were internalized into the cells possibly by endocytosis.⁴⁴ Notably, no morphological damage to the cells and more uptake number to the conjugates were observed even after co-incubation for 48 h, suggesting good biocompatibility of the CDs-COOH@PEA-NFAP conjugates. Therefore, the results indicate that the CDs-COOH@PEA-NFAP conjugates are desirable candidates for luminescence nanoplatforams for long-playing targeted biological therapy or drug delivery.

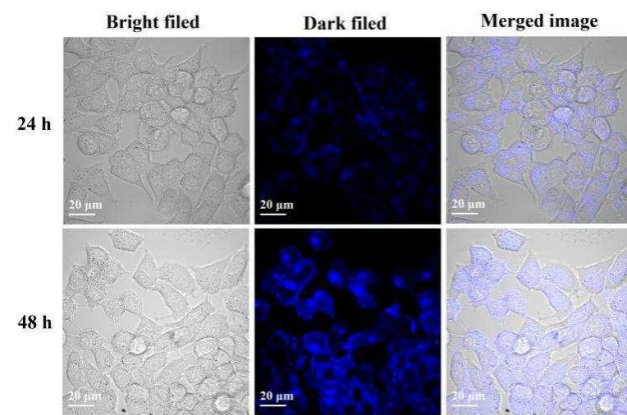


Figure 7. Confocal imaging of MCF-7 breast cancer cells incubated with CDs-COOH@PEA-NFAP conjugates with a concentration of $100 \mu\text{g mL}^{-1}$ for 24 h and 48 h at 37°C . Bright-field image (left); fluorescent images excited with a 405 nm laser (middle); merged image of bright-field image and fluorescent images (right).

Conclusions

For the first time, green type nanoplatforams based on carboxylic acid terminated CDs conjugating with amino terminated F-substituted hydroxyapatite (HAP) nanorods were successfully assembled. The bio-nanoplatforams combine the advantages of both the CDs and HAP and exhibit synergetic properties, such as well solubility in water, superior fluorescence and outstanding biocompatibility. The as-synthesized CDs-COOH@PEA-NFAP conjugates display excellent photostability compared to fluorescein isothiocyanate, CdTe QDs and Rhodamine B and strong colloidal stability in Tris-HCl buffer. Benefiting from the non-cytotoxicity and biocompatibility of the CDs and NFAP as verified by a series of standard methyl thiazolyl tetrazolium (MTT) assays with three different cell lines (MCF-7, HepG2, Caco-2), the CDs-COOH@PEA-NFAP conjugates show effective fluorescence performance for MCF-7 breast cancer cell imaging *in vitro* at UV light excitation. Coupled with biomolecules or anticancer drugs, the bio-nanoplatforams will provide targeted diagnostics and therapy in future. Thus, the rationally designed strategy may open up potential perspectives for multi-functional luminescent materials used in biological and biomedical applications.

Acknowledgements

This work was financially sponsored by Natural Science Foundation of Shanghai (13ZR1415100, 15ZR1415100) and the Science and Technology Commission of Shanghai Municipality (13JC1402700). We are also grateful to Instrumental Analysis & Research Center of Shanghai University.

Notes and references

- S. Zhu, Q. Meng, L. Wang, J. Zhang, Y. Song, H. Jin, K. Zhang, H. Sun, H. Wang and B. Yang, *Angew. Chem. Int. Ed.*, 2013, **52**, 3953-3957.
- B. C. Martindale, G. A. Hutton, C. A. Caputo and E. Reisner, *J. Am. Chem. Soc.*, 2015, **137**, 6018-6025.
- H. Nie, M. Li, Q. Li, S. Liang, Y. Tan, L. Sheng, W. Shi and S. X.-A. Zhang, *Chem. Mater.*, 2014, **26**, 3104-3112.
- L.-H. Xiong, R. Cui, Z.-L. Zhang, X. Yu, Z. Xie, Y.-B. Shi and D.-W. Pang, *ACS nano*, 2014, **8**, 5116-5124.
- B. H. Jun, D. W. Hwang, H. S. Jung, J. Jang, H. Kim, H. Kang, T. Kang, S. Kyeong, H. Lee, D. H. Jeong, K. W. Kang, H. Youn, D. S. Lee and Y. S. Lee, *Adv. Funct. Mater.*, 2012, **22**, 1843-1849.
- Y. Zhang, Y. Li and X.-P. Yan, *Anal. chem.*, 2009, **81**, 5001-5007.
- Y. Zhang, Y. Li and X. P. Yan, *Small*, 2009, **5**, 185-189.
- Q. Yang, K. Tang, C. Wang, Y. Qian and S. Zhang, *J. Phys. Chem. B.*, 2002, **106**, 9227-9230.
- R. Gill, M. Zayats and I. Willner, *Angew. Chem. Int. Ed.*, 2008, **47**, 7602-7625.
- U. Resch-Genger, M. Grabolle, S. Cavaliere-Jaricot, R. Nitschke and T. Nann, *Nat. Methods.*, 2008, **5**, 763-775.
- X. Wu, H. Liu, J. Liu, K. N. Haley, J. A. Treadway, J. P. Larson, N. Ge, F. Peale and M. P. Bruchez, *Nat. biotechnol.*, 2003, **21**, 41-46.
- S. Y. Lim, W. Shen and Z. Gao, *Chem. Soc. Rev.*, 2015, **44**, 362-381.

- 13 P. Anilkumar, X. Wang, L. Cao, S. Sahu, J.-H. Liu, P. Wang, K. Korch, K. N. Tackett II, A. Parenzan and Y.-P. Sun, *Nanoscale*, 2011, **3**, 2023-2027.
- 14 Y. Sun, F. Lu, X. Wang, L. Cao, Y. Lin, M. J. Mezziani, H. Wang, P. G. Luo, B. Zhou and B. A. Harruff, *NanoScience in Biomedicine*, Springer, 2009, pp. 128-153.
- 15 Z. Yang, M. Xu, Y. Liu, F. He, F. Gao, Y. Su, H. Wei and Y. Zhang, *Nanoscale*, 2014, **6**, 1890-1895.
- 16 K. Jiang, S. Sun, L. Zhang, Y. Lu, A. Wu, C. Cai and H. Lin, *Angew. Chem. Int. Ed.*, 2015, **54**, 5360-5363.
- 17 D. H. He, C. B. Zheng, Q. Wang, C. L. He, Y. I. Lee, L. Wu and X. D. Hou, *Talanta*, 2015, **142**, 51-56.
- 18 H. Ding, F. Du, P. Liu, Z. Chen and J. Shen, *ACS Appl. Mater. Interfaces*, 2015, **7**, 6889-6897.
- 19 X. Feng, Y. Jiang, J. Zhao, M. Miao, S. Cao, J. Fang and L. Shi, *RSC Adv.*, 2015, **5**, 31250-31254.
- 20 Z. Yang, M. Xu, Y. Liu, F. He, F. Gao, Y. Su, H. Wei and Y. Zhang, *Nanoscale*, 2014, **6**, 1890-1895.
- 21 L. Zhao, F. Di, D. Wang, L. H. Guo, Y. Yang, B. Wan and H. Zhang, *Nanoscale*, 2013, **5**, 2655-2658.
- 22 M. Vallet-Regí and J. M. González-Calbet, *Prog. Solid State Chem.*, 2004, **32**, 1-31.
- 23 J. Hui, G. Xiang, X. Xu, J. Zhuang and X. Wang, *Inorg. chem.*, 2009, **48**, 5614-5616.
- 24 J. Hui and X. Wang, *Chemistry*, 2011, **17**, 6926-6930.
- 25 Y. Liu, W. Wang, Y. Zhan, C. Zheng and G. Wang, *Mater. Lett.*, 2002, **56**, 496-501.
- 26 T. Takagahara and K. Takeda, *Phy. Rev. B.*, 1992, **46**, 15578.
- 27 L. A. Hails, J. C. Babister, S. Inglis, S. A. Davis, R. O. Oreffo and S. Mann, *Small*, 2010, **6**, 1986-1991.
- 28 D. Li, D. Jiang and J. Xie, *RSC Adv.*, 2015, **5**, 12392-12396.
- 29 K. L. Lin, X. G. Liu, J. Chang and Y. J. Zhu, *Nanoscale*, 2011, **3**, 3052-3055.
- 30 C. M. Curtin, G. M. Cunniffe, F. G. Lyons, K. Bessho, G. R. Dickson, G. P. Duffy and F. J. O'Brien, *Adv. Mater.*, 2012, **24**, 749-754.
- 31 H. Zhao, H. Zhou, J. Zhang, W. Zheng and Y. Zheng, *Biosens. Bioelectron.*, 2009, **25**, 463-468.
- 32 W. Y. Zhou, S. H. Lee, M. Wang, W. L. Cheung and W. Y. Ip, *J. Mater. Sci.-Mater. Med.*, 2008, **19**, 2535-2540.
- 33 L. Li, H. Pan, J. Tao, X. Xu, C. Mao, X. Gu and R. Tang, *J. Mater. Chem.*, 2008, **18**, 4079-4084.
- 34 J. Di Chen, Y. J. Wang, K. Wei, S. H. Zhang and X. T. Shi, *Biomaterials*, 2007, **28**, 2275-2280.
- 35 F.-H. Liu, Y.-K. Shen and J.-L. Lee, *Int. J. Precis. Eng. Man.*, 2012, **13**, 439-444.
- 36 H. Sun, F. Z. Su, J. Ni, Y. Cao, H. Y. He and K. N. Fan, *Angew. Chem. Int. Ed.*, 2009, **48**, 4390-4393.
- 37 M. Liu, H. Liu, S. Sun, X. Li, Y. Zhou, Z. Hou and J. Lin, *Langmuir*, 2014, **30**, 1176-1182.
- 38 S. Zhang, X. Zhao, H. Niu, Y. Shi, Y. Cai and G. Jiang, *J. Hazard. Mater.*, 2009, **167**, 560-566.
- 39 M.-F. Hsieh, J. K.-J. Li, C.-A. J. Lin, S.-H. Huang, R. A. Sperling, W. J. Parak and W. H. Chang, *J. Nanosci. Nanotechnol.*, 2009, **9**, 2758-2762.
- 40 R. Zhou, M. Li, S. Wang, P. Wu, L. Wu and X. Hou, *Nanoscale*, 2014, **6**, 14319-14325.
- 41 L. Zhang, J. Xia, Q. Zhao, L. Liu and Z. Zhang, *Small*, 2010, **6**, 537-544.
- 42 X. Wang, J. Zhuang, Q. Peng and Y. D. Li, *Adv. Mater.*, 2006, **18**, 2031-2034.
- 43 Y. Liu, N. Xiao, N. Gong, H. Wang, X. Shi, W. Gu and L. Ye, *Carbon*, 2014, **68**, 258-264.
- 44 P. C. Hsu and H. T. Chang, *Chem. Commun.*, 2012, **48**, 3984-3986.
- 45 L. Yang, W. Jiang, L. Qiu, X. Jiang, D. Zuo, D. Wang and L. Yang, *Nanoscale*, 2015, **7**, 6104-6113.
- 46 X. Cui, L. Zhu, J. Wu, Y. Hou, P. Wang, Z. Wang and M. Yang, *Biosens. bioelectron.*, 2015, **63**, 506-512.
- 47 Q. Cai, J. F. Mao, X. L. Li and X. P. Yang, *Mater. Lett.*, 2014, **128**, 238-241.
- 48 G. Hannink, P. J. Geutjes, W. F. Daamen and P. Buma, *J. Mater. Sci.: Mater. Med.*, 2013, **24**, 325-332.
- 49 L. Yang, W. H. Jiang, L. P. Qiu, X. W. Jiang, D. Y. Zuo, D. K. Wang and L. Yang, *Nanoscale*, 2015, **7**, 6104-6113.